Cellular/Molecular

Photoreceptor Coupling Is Controlled by Connexin 35 Phosphorylation in Zebrafish Retina

Hongyan Li,[1] Alice Z. Chuang,[1] and John O'Brien[1,2]

[1]Department of Ophthalmology and Visual Science and [2]Graduate School of Biomedical Sciences, The University of Texas Health Science Center at Houston, Houston, Texas 77030

Electrical coupling of neurons is widespread throughout the CNS and is observed among retinal photoreceptors from essentially all vertebrates. Coupling dampens voltage noise in photoreceptors and rod–cone coupling provides a means for rod signals to enter the cone pathway, extending the dynamic range of rod-mediated vision. This coupling is dynamically regulated by a circadian rhythm and light adaptation. We examined the molecular mechanism that controls photoreceptor coupling in zebrafish retina. Connexin 35 (homologous to Cx36 of mammals) was found at both cone–cone and rod–cone gap junctions. Photoreceptors showed strong Neurobiotin tracer coupling at night, extensively labeling the network of cones. Tracer coupling was significantly reduced in the daytime, showing a 20-fold lower diffusion coefficient for Neurobiotin transfer. The phosphorylation state of Cx35 at two regulatory phosphorylation sites, Ser110 and Ser276, was directly related to tracer coupling. Phosphorylation was high at night and low during the day. Protein kinase A (PKA) activity directly controlled both phosphorylation state and tracer coupling. Both were significantly increased in the day by pharmacological activation of PKA and significantly reduced at night by inhibition of PKA. The data are consistent with direct phosphorylation of Cx35 by PKA. We conclude that the magnitude of photoreceptor coupling is controlled by the dynamic phosphorylation and dephosphorylation of Cx35. Furthermore, the nighttime state is characterized by extensive coupling that results in a well connected cone network.

Introduction

Electrical coupling of neurons has emerged as a fundamental component of CNS wiring (Connors and Long, 2004). The vertebrate retina has long been the premier model system in which to study electrical synapses. Evidence that vertebrate photoreceptors are electrically coupled emerged from some of the earliest intracellular recordings (Tomita et al., 1967; Baylor et al., 1971). Ultrastructural observations showed that photoreceptors make small gap junctions, the substrate for electrical coupling, among synaptic terminals and telodendrial processes. These gap junctions are nearly ubiquitously present between cones and between rods and cones in vertebrate retina (Raviola and Gilula, 1973, 1975; Witkovsky et al., 1974; Kolb, 1977; Gold and Dowling, 1979; Cooper and McLaughlin, 1981). Nearly all of these gap junctions have been demonstrated to be formed by connexin 35 (O'Brien et al., 2004; Zhang and Wu, 2004; Kihara et al., 2009) or its mammalian homolog Cx36 (Deans et al., 2002; Dang et al., 2004; Degen et al., 2004), although small Cx34.7 gap junctions are present in bass cones along with Cx35 (O'Brien et al., 2004) and an unidentified connexin may be present on the rod side of rod–cone gap junctions in guinea pig (Lee et al., 2003).

The functional significance of electrical coupling in retina has been extensively studied. Cell–cell coupling improves the signal-to-noise ratio of the photovoltage response (Lamb and Simon, 1976), although necessarily at the cost of signal amplitude and modest blurring of focal signals (Schneeweis and Schnapf, 1999; DeVries et al., 2002). Rod–cone coupling also allows signals in rod and cone pathways to mix (Schwartz, 1975; Nelson, 1977; Schneeweis and Schnapf, 1995; Trümpler et al., 2008). This crossover provides a medium-sensitivity pathway that may operate under mesopic light intensities when the primary high-sensitivity rod pathway becomes saturated (DeVries and Baylor, 1995; Völgyi et al., 2004).

Regulation of rod–cone coupling plays a critical role in light and dark adaptation. In teleost fish and mammals, the conductance of rod–cone gap junctions is regulated by a circadian rhythm that reduces rod input to cones during the subjective day (Wang and Mangel, 1996; Ribelayga et al., 2008); photopic light adaptation also triggers this response. A variety of data implicates the action of dopamine, via D_4 or D_2-like receptors, in imposing the daytime or light-adapted state on photoreceptors (Hillman et al., 1995; Krizaj et al., 1998; Nir et al., 2002; Ribelayga et al., 2008). When activated this pathway functions by inhibition of adenylyl cyclase and reduction of cAMP (Cohen et al., 1992).

In vitro and cell culture studies have shown that Cx35 can be phosphorylated by cAMP-dependent protein kinase (PKA) (see Fig. 1) and that phosphorylation regulates coupling (O'Brien et al., 2004; Ouyang et al., 2005). These observations suggest that the

Received June 15, 2009; revised Oct. 14, 2009; accepted Oct. 19, 2009.

This work was supported by the American Health Assistance Foundation Macular Degeneration Research program, National Institutes of Health Grants EY12857 and EY10608, and Research to Prevent Blindness. We thank W. Wade Kothmann and Dr. Steven Wang for assistance with superfusion experiments and microscopy and Dr. Cristophe Ribelayga for helpful comments on this manuscript.

Correspondence should be addressed to John O'Brien, Department of Ophthalmology and Visual Science, The University of Texas Health Science Center at Houston, 6431 Fannin Street, MSB 7.024, Houston, TX 77030. E-mail: john.obrien@uth.tmc.edu.

DOI:10.1523/JNEUROSCI.3517-09.2009

 0270-6474/09/2915178-09$15.00/0

changes in photoreceptor coupling caused by the circadian rhythm and light adaptation could be caused by PKA-mediated phosphorylation of Cx35. In this study, we examined the molecular mechanism that regulates photoreceptor coupling and found that Cx35 phosphorylation is directly correlated with changes in coupling and that PKA activity plays a central role in controlling phosphorylation state.

Materials and Methods

Tracer coupling measurements. Wild-type, AB-strain adult zebrafish were used in the current study. All procedures performed on animals were approved by the institutional animal care and use committee. Zebrafish were maintained on a 12 h light/dark cycle for at least 2 weeks before experiments. Fish were anesthetized with 0.15% tricaine (Sigma-Aldrich) and their spinal cords transected behind the head. Eyes were dissected and the anterior segment and lens removed to produce an eyecup preparation. Nighttime studies, conducted in darkness or under infrared light, were initiated 4 h before light onset and completed 2 h before light onset. Daytime studies were conducted under photopic illumination and initiated 2 h after light onset. The night–day transitions were avoided to reduce variability caused by circadian rhythm-induced transitions in photoreceptor coupling (Wang and Mangel, 1996).

We examined gap junction coupling between photoreceptors by measuring diffusion of Neurobiotin (Vector Laboratories) between photoreceptors using a cut loading technique (Ribelayga et al., 2008). Changes in tracer coupling have been found to correlate with changes in receptive field properties of well coupled neurons (Bloomfield et al., 1995, 1997), so this measure is thought to reflect electrical coupling in the network. Whole-mount retinas were prepared from zebrafish eyecups and incubated for 30 min in oxygenated modified Ames' solution (United States Biological; stock Ames' medium plus 10 mM HEPES and 12 mM $NaHCO_3$, pH 7.4). For some daytime retinas, 20 μM PKA activator Sp-8-cpt-cAMPS (Axxora) was added to the bath and was present in the following steps until fixation; some nighttime retinas were treated similarly with 20 μM PKA inhibitor Rp-8-cpt-cAMPS (Axxora). Radial cuts were made with a double-sided razor dipped in 5% Neurobiotin freshly made with oxygenated modified Ames' solution. The retinas were subsequently incubated with 0.1% Neurobiotin in oxygenated modified Ames' medium for 15 min and washed in medium without Neurobiotin. Retina tissue was fixed in 4% formaldehyde in 0.1 M phosphate buffer, pH 7.4, for 1 h, washed with PBST (PBS plus 0.5% Triton X-100, 0.1% NaN_3), and incubated with 1:500 Cy3-conjugated streptavidin (Jackson ImmunoResearch) at 10°C overnight. Whole-mount view images at the level of photoreceptor inner segments were digitally captured using a Zeiss LSM 510 Meta confocal microscope with similar settings of pinhole, contrast, and brightness parameters. All cut loading experiments under each condition were conducted on 3–5 separate days and sampled from at least five animals.

The fluorescence intensity of Cy3-streptavidin-labeled Neurobiotin was measured in 4-μm-diameter circles centered on photoreceptor inner segments using SimplePCI software (Compix). The mean cell-to-cell spacing was also measured in the same images. Data were collected primarily from cones, although it is possible that, in these low-magnification images, some data from rods were included in the datasets. No distinction was made among cone types.

The diffusion of Neurobiotin between coupled photoreceptors was estimated using a linear compartmental diffusion model (Zimmerman and Rose, 1985) as applied to neural networks by Mills and colleagues (Mills and Massey, 1998; O'Brien et al., 2004). This model treats the array of neurons as a linear chain of compartments connected by identical gap junctions characterized by a rate-limiting diffusion coefficient (k). The k parameter represents the proportion of the tracer that diffuses from one compartment to the adjacent compartment in 1 s. Tracer loaded into the first compartment moves into subsequent compartments based on the concentration difference between those compartments. The linear configuration is formally equivalent to a square array of cells connected to four nearest neighbors by gap junctions when one applies the simplifying assumptions that all cells along the cut edge are loaded equally and that the cut edge follows one edge of the array.

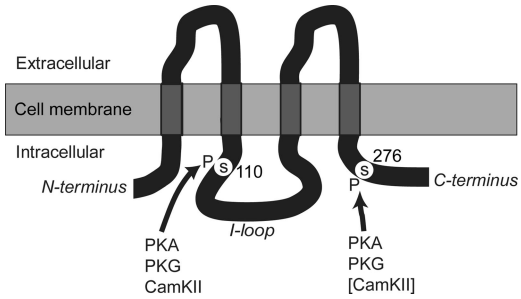

Figure 1. Schematic representation of connexin 35 regulation. Two major phosphorylation sites, serine-110 in the intracellular loop and serine-276 in the C terminus, play critical roles in controlling cell coupling through Cx35 gap junctions. Phosphorylation of both sites is required to achieve full regulation of coupling (Ouyang et al., 2005). Several protein kinases phosphorylate these sites including PKA, PKG, and CaMKII (Ca^{2+}/calmodulin-dependent protein kinase II). The two sites are not equivalent and protein kinases phosphorylate them with differing efficacies.

To apply the model, plots of the fluorescence intensity versus distance from the cut edge in cell-to-cell spacings were fit to the diffusion model by varying the diffusion coefficient (k) and tracer injection rate (bo) parameters (see supplemental Fig. 1, available at www.jneurosci.org as supplemental material). Optimal fits of the intensity data to the model were determined using MatLab (Mathworks). Since the model is linear and presumes that loading occurs in a single compartment, we performed the analysis among a narrow cluster of cells extending perpendicular to the cut edge. Diffusion coefficients were compared under different conditions using a two-sample t test.

Antibodies used for immunocytochemistry. Two phosphospecific anti-Cx35 antibodies were used to measure phosphorylation of Cx35 at its two primary regulatory phosphorylation sites (Fig. 1). These antibodies specifically label the phosphorylated Ser110 and Ser276 sites of Cx35 as well as the equivalent sites (Ser110 and Ser293) of Cx36 (Kothmann et al., 2007). In all experiments, Cx35 was also labeled with a monoclonal antibody to perch Cx35 (anti-Cx35/36; clone 8F6.2; Millipore). Monoclonal antibodies against synaptic vesicle protein 2 (SV2) were obtained from the Developmental Studies Hybridoma Bank. The monoclonal antibody FRet43 (aka ZPR1), which labels zebrafish double cone membranes (Larison and Bremiller, 1990), was obtained from the University of Oregon Zebrafish International Resource Center (Eugene, OR). A rabbit polyclonal anti-goldfish syntaxin 3 antibody was generously provided by Dr. Roger Janz (Department of Neurobiology and Anatomy, University of Texas Health Science Center at Houston, Houston, TX). Cy3- and Cy5-conjugated secondary antibodies were obtained from Jackson ImmunoResearch; Alexa-488 conjugated secondary antibodies were from Invitrogen.

Sequential immunocytochemistry. Eyecups were prepared as above, then washed in PBS and fixed with 4% formaldehyde in 0.1 M phosphate buffer, pH 7.4, for 45 min. The fixed eyecups were washed with PBS and cryoprotected by immersion in 30% sucrose at 4°C overnight. Eyecups were embedded in Tissue-Tek OCT compound (Sakura Finetek), frozen at −20°C, and cut into 20 μm sections with a cryostat.

We wanted to demonstrate morphologically the relationship between Cx35 and photoreceptors. Since both SV2 and FRet43 are mouse IgG antibodies, and each of them was to be used together with mouse anti-Cx35/36 monoclonal antibody, we used a sequential labeling technique. Eyecup sections were rehydrated in PBST and blocked in 10% normal donkey serum (Jackson ImmunoResearch) in PBST for 1 h at room temperature. Sections were incubated with 2.5 μg/ml anti-Cx35/36 in 5% donkey serum at 4°C overnight. Tissue sections were washed in PBST and then incubated with Alexa 488-conjugated donkey anti-mouse IgG (5 μg/ml; Invitrogen) in 5% donkey serum at room temperature for 7 h. After washing with PBST, sections were incubated with 140 μg/ml Fab fragment goat anti-mouse IgG (Jackson ImmunoResearch) in 5% donkey serum at 4°C overnight. On the next day, tissue was extensively

washed with PBST and subsequently incubated with FRet43 (dilution, 1:20) or mouse anti-SV2 (dilution, 1:1000) in 5% donkey serum at 4°C overnight. Then tissue sections were washed in PBST and incubated with Cy3-conjugated donkey anti-mouse IgG (3.75 μg/ml; Jackson ImmunoResearch) or Cy5-conjugated donkey anti-mouse IgG (3.5 μg/ml; Jackson ImmunoResearch), respectively, for 2 h at room temperature. Plasma membranes of rod spherules and cone pedicles were labeled with anti-syntaxin 3 (dilution, 1:100) at 4°C overnight, followed by 2 h incubation with Cy3-conjugated donkey anti-rabbit IgG (3.7 μg/ml; Jackson ImmunoResearch) at room temperature. After washing in PBST, sections were mounted with Vectashield (Vector Laboratories). Images were taken with the confocal microscope.

Retina superfusion and immunocytochemistry. These studies were either finished by 2 h before light onset (night) or begun 2 h after light onset (day) as described above. Once eyecups were prepared as described above, they were superfused with oxygenated modified Ames' medium or modified Ames' containing 20 μM PKA activator Sp-8-cpt-cAMPS or 20 μM PKA inhibitor Rp-8-cpt-cAMPS for 30 min. After superfusion, eyecups were fixed for 30 min with 1% *N*-(3-dimethylaminopropyl)-*N*′-ethylcarbodiimide hydrochloride (Sigma-Aldrich) in fixation buffer (116 mM Tris, 68 mM NaCl, 1.3 mM KCl, 52 mM Na_2HPO_4, 25 mM NaH_2PO_4, 0.9 mM KH_2PO_4, pH 7.5). Eyecups were then washed in PBS, cryoprotected in 30% sucrose overnight, embedded, and cryostat sectioned as described above.

Eyecup sections were rehydrated in PBST and blocked in 10% normal donkey serum in PBST for 1 h at room temperature. The primary antibodies were prepared as a mixture in 5% donkey serum with PBST containing 2.5 μg/ml mouse anti-Cx35/36 and 0.8 μg/ml rabbit anti-phospho-Ser110 or 1 μg/ml anti-phospho-Ser276 (Kothmann et al., 2007). Sections were incubated with the primary antibodies overnight at 4°C. The sections were washed in PBST and incubated with the two secondary antibodies, Cy3-conjugated donkey anti-mouse IgG (0.9 μg/ml) and Alexa 488-conjugated donkey anti-rabbit IgG (1.25 μg/ml), for 2 h at room temperature.

Image acquisition and phosphorylation state analysis. Image acquisition and data analysis were conducted as described previously (Kothmann et al., 2007). Immunostaining was imaged on the confocal microscope using 12 bit data acquisition. Images of each phospho-antibody and Cx35 signals were taken at standardized settings to facilitate comparison of labeling between different lighting conditions or drug treatments. Five confocal slices at 0.3 μm intervals were taken at randomly selected locations in the outer plexiform layer (OPL) in the region from 50 to 80% of the distance from the optic nerve head to the periphery. Three neighboring slices were stacked to generate a 12 bit tiff image with the brightest pixel intensity slightly saturated so that the intensity of the majority of pixels fell in the linear range of the intensity curve. Five images were collected for each eyecup, with images distributed among three to four sections. Each eyecup was collected from a different animal and at least five animals were sampled for each experimental condition.

Images were analyzed with SimplePCI software. Regions of interest (ROIs), equivalent to single Cx35 gap junctions, were selected based on signals of Cx35 monoclonal immunolabeling and defined as contiguous pixels whose Cx35 intensity was >20% of the total intensity range and whose size was no smaller than 0.1 μm^2. For each ROI, intensity in both Cx35 and phospho-antibody channels was obtained. Cx35 phosphorylation was expressed as the ratio of phospho-antibody channel intensity to Cx35 channel intensity. The distribution of intensity ratios of all gap junctions in the five images for each eye was examined for normality using a Kolmogorov–Smirnov test with R software, version 2.9.1 (www.r-project.org). Since these values were not normally distributed (see Fig. 5*A*,*B*), the median intensity ratio was calculated for each animal to generate a single value representing the phosphorylation state of the OPL in one animal. The median values for three to six animals under each condition were compared using a two-sample *t* test and are expressed as the means of the individual sample median values.

A second measurement of phosphorylation state was made by calculating the fraction of Cx35 gap junctions that had any detectable phosphorylation. The threshold for detectable phosphorylation was defined as intensity in the phospho-antibody channel that was 150% of the average value of the background labeling in that channel in areas with no Cx35 gap junctions. The fraction of phosphorylated gap junctions was calculated for each image and the mean value was calculated for the five images from each eyecup. The mean values were compared using a two-sample *t* test.

Results

Cx35 gap junctions are located between photoreceptors

Connexin35 has been identified in cone photoreceptors in bass retina using *in situ* hybridization and immunocytochemistry (O'Brien et al., 2004). In keeping with this observation, high-magnification images taken in the zebrafish OPL revealed numerous Cx35 plaques, most of which were associated with cone photoreceptor terminals (Fig. 2*A*,*B*). On FRet43-labeled double cone photoreceptors, many Cx35 gap junctions occurred on telodendria and contacts between neighboring cones (Fig. 2*A*,*B*, arrowheads). These are interpreted to represent cone–cone gap junctions between the double cones. Cx35 was also observed on and above double cone pedicles, most likely forming gap junctions with unresolved telodendria, terminals or processes of the two unlabeled types of cone photoreceptors, and with rods. The Cx35 gap junctions at the base of each cone pedicle may also include gap junctions among bipolar cells, as this type of gap junction has been observed in carp retina (Cuenca et al., 1993) and numerous small gap junctions observed ultrastructurally in the OPL of mammalian retina may also include bipolar cell gap junctions (Raviola and Gilula, 1975).

To determine whether Cx35 above cone pedicles formed rod–rod or rod–cone gap junctions, we examined the retina with a combination of antibodies against syntaxin 3 and synaptic vesicle protein 2 (Fig. 2*C*–*F*). Both antibodies label all photoreceptor terminals and the combination provided a clear outline of rod spherules. In contrast to cone pedicles, rod spherules mainly resided at a higher level of the OPL. Many Cx35 gap junctions were associated with rod spherules and colocalized with the plasma membrane marker syntaxin 3 (Fig. 2*C*,*D*, arrows). Some Cx35 was clearly localized between a rod spherule and a cone pedicle (Fig. 2*E*,*F*, arrowheads). Thus, our data suggest that Cx35 is involved in both cone–cone and rod–cone gap junctions in zebrafish retina. It was not clear whether any of the Cx35 represented rod–rod gap junctions.

Time of day changes photoreceptor coupling and the phosphorylation state of Cx35 gap junctions

Gap junctional coupling of rods to cones is controlled by a circadian rhythm. In several species, there is significant rod input to cones and downstream neurons at night, but not during the day (Wang and Mangel, 1996; Ribelayga et al., 2008). This electrical coupling is reflected in extensive tracer coupling among rods and cones at night in both goldfish and mouse (Ribelayga et al., 2008). To examine whether zebrafish retina followed the pattern observed in other species, we performed tracer coupling experiments in isolated zebrafish retina using the cut loading technique (Ribelayga et al., 2008). At night under fully dark-adapted conditions, tracer coupling among photoreceptors was extensive and labeled cones >100 μm from the cut edge of the retina after 20 min of diffusion (Fig. 3*A*). In contrast, tracer diffusion was much less in light-adapted conditions during the day (Fig. 3*B*). To analyze these data quantitatively, we fit the fluorescence intensity of tracer-filled photoreceptors to a compartmental diffusion model (supplemental Fig. 1, available at www.jneurosci.org as supplemental material). From this fit, we calculated a diffusion coeffi-

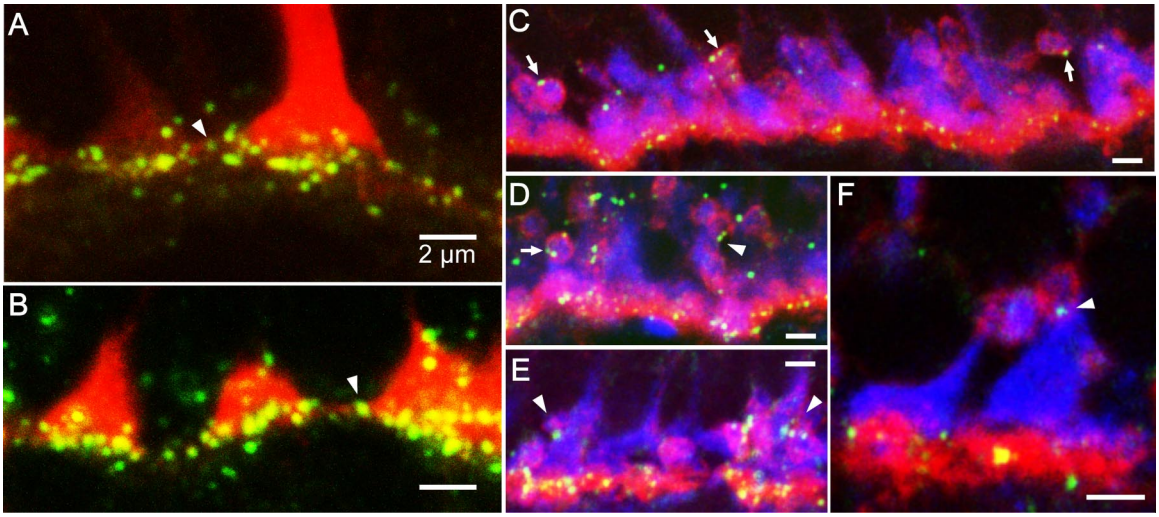

Figure 2. Localization of connexin 35 in zebrafish OPL. ***A***, ***B***, Cx35 gap junctions (green) are abundantly associated with double cone pedicles and telodendria, labeled with antibody FRet43 (red; note that long and short single cones are not labeled). Some Cx35 can be seen at points of contact between cone pedicles and telodendria from adjacent cones (arrowheads). There are numerous Cx35 plaques beneath each pedicle, which may constitute cone– cone or bipolar cell gap junctions. Also, many Cx35 gap junctions occur on upper portions of the pedicles, possibly providing contacts with rods. ***C–F***, Labeling all rod and cone terminals with a combination of antibodies against syntaxin3 (red) and SV2 (blue) provides more information about the rod– cone contacts. Small Cx35 gap junctions (green) are closely associated with rod spherules (arrows). In some circumstances, Cx35 gap junctions are found between a rod spherule and a cone pedicle (***D–F***, arrowheads). Scale bar, 2 μm.

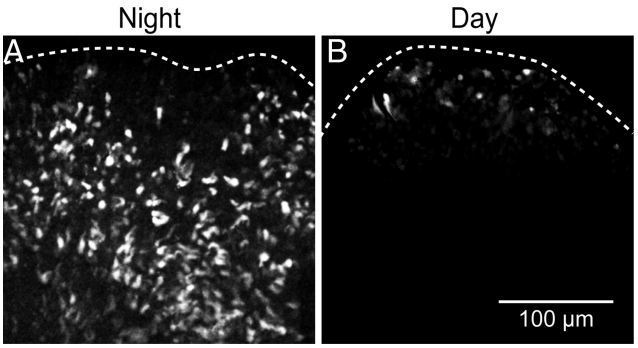

Figure 3. Photoreceptor coupling in the night and day. ***A***, Cut loading of Neurobiotin at night in darkness yielded extensive tracer diffusion through the photoreceptor matrix from the cut edge (dashed line). Most photoreceptors visible in the images are cones. ***B***, In contrast, tracer diffusion was much more limited in the daytime under light-adapted conditions.

cient (k) for Neurobiotin spread through the photoreceptor network. Comparison of diffusion coefficients indicated that gap junctions between photoreceptors had significantly lower permeability in the daytime compared with the nighttime (night: $k = 0.0043 \pm 0.0019$ cells^2/s, $n = 5$ animals; day: $k = 0.0002 \pm 0.0001$ cells^2/s, $n = 6$ animals; $p = 0.04$). Thus, zebrafish photoreceptor coupling followed the pattern observed in mammalian and other teleost photoreceptor networks (Ribelayga et al., 2008).

In previous experiments in cell culture expression systems, we found that tracer coupling is controlled by phosphorylation of two critical regulatory sites on Cx35: Ser110 and Ser276 (Ouyang et al., 2005; Patel et al., 2006). To understand the relationship between photoreceptor coupling and Cx35 phosphorylation, we examined the phosphorylation state of both sites using phosphospecific antibodies (Kothmann et al., 2007). At night in darkness, Cx35 gap junctions in the OPL exhibited variable amounts of phosphorylation at Ser110 (Fig. 4*A*) and at Ser276 (Fig. 4*B*). Under light-adapted conditions in the daytime, phosphorylation was greatly reduced at both sites, although a small number of gap junctions retained substantial phosphorylation (Fig. 4*C*,*D*).

To measure phosphorylation of the OPL gap junctions quantitatively, we expressed phosphorylation state as the ratio of phospho-Cx35 Ab labeling intensity to Cx35 monoclonal Ab labeling intensity on each individual gap junction. Figure 5 shows that, within a single sample, phosphorylation states were distributed over a wide range of values. The distribution included more gap junctions at higher values at night (Fig. 5*A*) than in the day (Fig. 5*B*). A test of normality indicated that the distribution of phosphorylation states within a single sample was not normal (see Materials and Methods). For this reason, we used the median phosphorylation state to characterize each sample. Figure 5*C* shows that the median phosphorylation state of OPL gap junctions was reduced in daytime compared with the nighttime retina, although significantly so only for Ser276 (S110 night: P110/Cx35 mean of three animals = 1.08; S110 day: P110/Cx35 mean of three animals = 0.36, $p = 0.17$; S276 night: P276/Cx35 mean of five animals = 0.59; S276 day: P276/Cx35 mean of six animals = 0.25, $p = 0.02$). When we analyzed the fraction of Cx35 gap junctions that showed any detectable phosphorylation (defined as >150% of the background in the phospho-Ab channel), we found that a significantly smaller fraction of Cx35 plaques showed phosphorylation in the daytime retina compared with the nighttime at both Ser110 and Ser276 sites (Fig. 5*D*) (S110 night: mean $f_{phos} = 0.70$, $n = 3$; S110 day: mean $f_{phos} = 0.30$, $n = 3$, $p < 0.01$; S276 night: mean $f_{phos} = 0.67$, $n = 5$; S276 day: mean $f_{phos} = 0.21$, $n = 6$, $p < 0.01$).

PKA activity regulates Cx35 phosphorylation and photoreceptor coupling

Light-induced changes in photoreceptor coupling can be partially mimicked by activating dopamine D_2/D_4 receptors (Krizaj et al., 1998; Ribelayga et al., 2008), which reduces adenylyl cyclase activity and cytoplasmic cAMP concentration and thus reduces PKA signaling (Dearry and Burnside, 1986; Cohen et al., 1992; Nir et al., 2002). Since both Ser110 and Ser276 are potential targets of PKA phosphorylation (Ouyang et al., 2005), we hypothesized that activating PKA in the daytime would convert the photoreceptor gap junctions to a nighttime-like state. To

test this hypothesis, we treated light-adapted retinas in daytime with Sp-8-cpt-cAMPS, a membrane-permeant cAMP analog that activates PKA. Figure 6*A* shows that this treatment increased Neurobiotin tracer coupling among photoreceptors, partially mimicking the nighttime condition. Quantitative evaluation of coupling showed that this increase was significant (day control: $k = 0.0003 \pm 0.0001$ cells^2/s, $n = 5$; Sp: $k = 0.0036 \pm 0.0009$ cells^2/s, $n = 6$; $p < 0.01$). In keeping with this observation, Sp treatment in the daytime increased Cx35 phosphorylation compared with control (Fig. 6*B*). Figure 6, *C* and *D*, shows that both the median ratio of phospho-Ab to Cx35 MAb and the fraction of phosphorylated Cx35 plaques were significantly increased for both Ser110 (intensity ratio: control: P110/Cx35 mean of five animals = 0.10; Sp: P110/Cx35 mean of five animals = 0.20, $p < 0.01$; fraction data: control: $f_{phos} = 0.14$; Sp: $f_{phos} = 0.46$, $p < 0.01$) and Ser276 (intensity ratio: control: P276/Cx35 mean of six animals = 0.04; Sp: P276/Cx35 mean of six animals = 0.08, $p < 0.05$; fraction data: control: mean $f_{phos} = 0.17$; Sp: mean $f_{phos} = 0.54$, $p < 0.01$).

In the nighttime, the cAMP level in photoreceptors is relatively high (Cohen and Blazynski, 1987; Nir et al., 2001) and should maintain a moderate level of PKA activity. If PKA phosphorylates Cx35 gap junctions in the nighttime, inhibiting PKA activity should resemble the daytime state and reduce Cx35 phosphorylation. Figure 7*A* shows that treatment with Rp-8-cpt-cAMPS, a membrane-permeant cAMP analog that inhibits PKA, reduced Neurobiotin tracer coupling among photoreceptors, replicating the daytime condition. This change was statistically significant (night control: $k = 0.0028 \pm 0.0006$ cells^2/s, $n = 5$; Rp: $k = 0.0004 \pm 0.0001$ cells^2/s, $n = 5$; $p < 0.01$). As predicted from the change in coupling, Rp treatment at night also reduced phosphorylation of Cx35 (Fig. 7*B*). Quantitative measurement shows that the median ratio of phospho-Ab to Cx35 MAb was significantly reduced for Ser276 (Fig. 7*C*) (S110 night: P110/Cx35 mean of six animals = 0.37; S110 night plus Rp: P110/Cx35 mean of six animals = 0.21, $p = 0.19$; S276 night: P276/Cx35 mean of six animals = 0.57, S276 night plus Rp: P276/Cx35 mean of four animals = 0.34, $p = 0.03$). The fraction of gap junctions detectably phosphorylated was significantly reduced for both Ser110 and Ser276 (Fig. 7*D*) (S110 night: mean $f_{phos} = 0.57$, $n = 6$; S110 night plus Rp: mean $f_{phos} = 0.14$, $n = 6$, $p < 0.01$; S276 night: mean $f_{phos} = 0.57$, $n = 6$; S276 night plus Rp: mean $f_{phos} = 0.32$, $n = 4$, $p = 0.02$). Thus, manipulation of PKA activity either in nighttime or daytime conditions is sufficient to change both the phosphorylation state and the coupling of photoreceptor gap junctions.

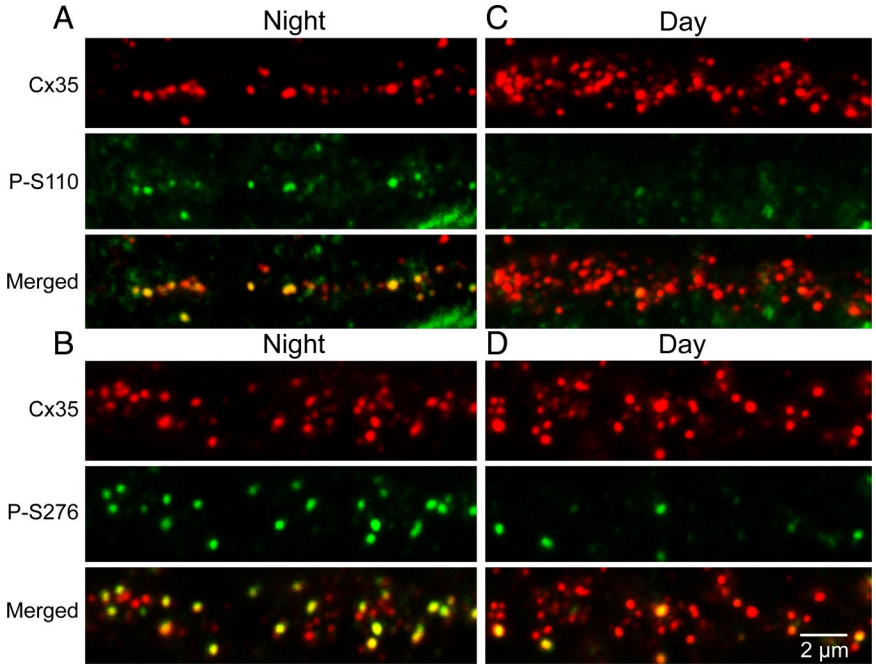

Figure 4. Phosphorylation state of Cx35 in the OPL in the night and day. Each panel shows phospho-Cx35 antibody labeling on Cx35 gap junctions in the OPL. Total Cx35, labeled with monoclonal anti-Cx35/36 (red), is displayed on top, phospho-Ser110 or phospho-Ser276 (green) in the center, and the merged image below. At night, Cx35 gap junctions showed substantial phosphorylation at both Ser110 (***A***) and Ser276 (***B***) sites. Less phosphorylation was evident in the daytime on Ser110 (***C***) and Ser276 (***D***).

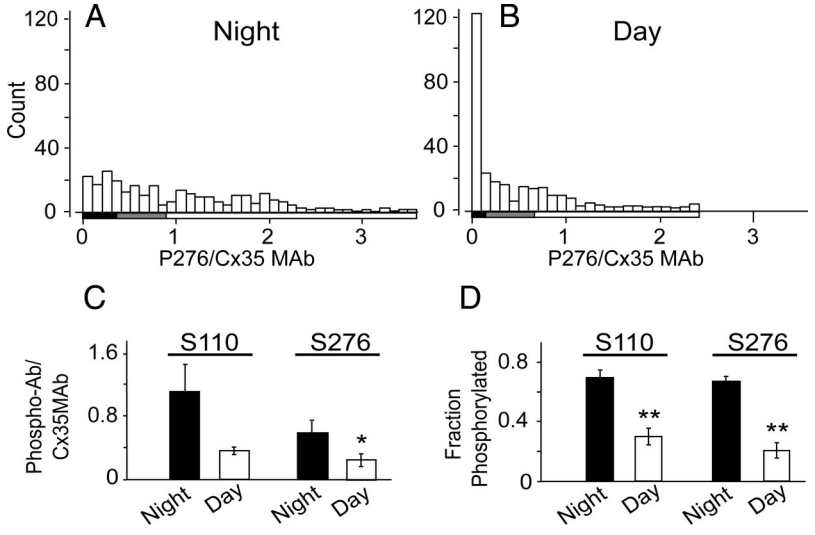

Figure 5. Quantitative analysis of Cx35 phosphorylation states in night and day. Distribution of the ratios of phospho-S276/Cx35 monoclonal Ab labeling intensities for individual gap junctions in one representative nighttime (***A***) and one representative daytime (***B***) retina. Data for each distribution are pooled from five images taken from three sections from each eye. Bin size is an intensity ratio of 0.1. The bars below each histogram map the intensity threshold (150% of background) used to calculate the fraction of gap junctions detectably phosphorylated. In the region denoted by the black bar, all gap junctions fall below this threshold; in the gray region, some gap junctions fall below the threshold and some are above the threshold. For quantitative comparisons, each animal was characterized by the median phospho-Cx35 Ab/Cx35 monoclonal Ab intensity ratio of the total population of OPL gap junctions (***C***) and the fraction of Cx35 gap junctions showing detectable phosphorylation (***D***). Both measures show daytime phosphorylation state to be reduced compared with nighttime. $N = 3$ animals per condition for Ser110; $n = 5$ for Ser276 night and $n = 6$ for Ser276 day. Error bars are ±SEM. *$p < 0.05$; **$p < 0.01$.

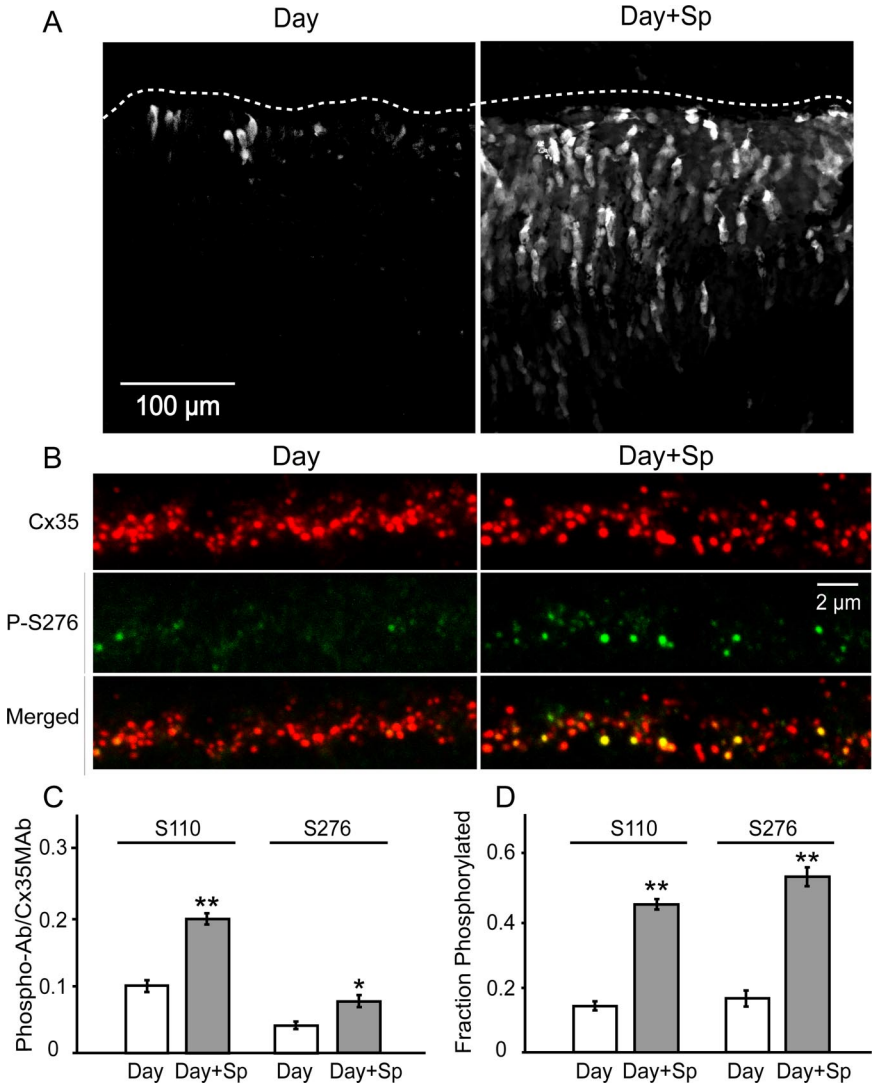

Figure 6. Activating PKA increases photoreceptor coupling and Cx35 phosphorylation in the daytime. Treatment with the PKA activator Sp-8-cpt-cAMPS (20 μM) during the daytime under photopic illumination increased the spread of Neurobiotin through the photoreceptor network (***A***). The dashed line indicates the cut edge of the retina. Sp treatment increased the labeling for phospho-Ser276 (***B***). Ser110 showed the same effects, resulting in significant increases in the median ratio of phospho-Cx35 Ab/Cx35 monoclonal Ab labeling intensity (***C***) and the fraction of Cx35 plaques phosphorylated (***D***) for both Ser110 and Ser276 ($n = 5$ for Ser110 in day and Sp conditions; $n = 6$ for Ser276 in day and Sp). Error bars are $\pm$SEM. $^*p < 0.05$; $^{**}p < 0.01$.

Discussion

Signaling mechanisms that control gap junction coupling

The visual experience of many vertebrate animals may span 10 log units of light intensity. A number of adaptation mechanisms come into play to allow some form of vision throughout this range. The transition from rod-mediated vision in the scotopic range to cone-mediated vision in the photopic range is a critical part of this process. A large body of evidence indicates that adenylyl cyclase/cAMP signaling pathways, driven in photoreceptors by adenosine at night and dopamine during the day, play an important role in this transition. The adaptive mechanisms in photoreceptors controlled by these pathways include opposing photomechanical movements of rods and cones (Dearry and Burnside, 1985; Pierce and Besharse, 1985; Dearry et al., 1990; Stenkamp et al., 1994; Rey and Burnside, 1999), modulation of calcium currents (Stella and Thoreson, 2000; Stella et al., 2002, 2003) and chloride currents (Thoreson et al., 2002), and changes in rod–cone (Yang and Wu, 1989; Krizaj et al., 1998; Ribelayga et al., 2008) and cone–cone (Copenhagen and Green, 1987) gap junctional coupling. The net effect of most of these adaptive changes is to reduce rod input and increase cone input to postreceptoral neurons during the day or when adapted to bright light (Witkovsky et al., 1988, 1989; Wang and Mangel, 1996; Ribelayga et al., 2002).

In this study, we examined the molecular mechanism that controls photoreceptor gap junctional coupling. In agreement with previous observations, a cAMP/protein kinase A signaling pathway controlled coupling. We found that photoreceptor coupling is directly related to Cx35 phosphorylation state at two residues, Ser110 and Ser276. Increased phosphorylation at these sites indicated increased coupling. In previous studies, we showed that these two residues are critical for regulation of cell-to-cell coupling by PKA activity and by the nitric oxide/cGMP-dependent protein kinase (PKG) signaling system (Ouyang et al., 2005; Patel et al., 2006), and Mitropoulou and Bruzzone (2003) showed the Ser110 site to be functionally required for cAMP regulation of gap junction hemichannel currents. These observations suggest that the Cx35 phosphorylation state controls coupling. Indeed, manipulating PKA activity in photoreceptors to increase Cx35 phosphorylation in the daytime or decrease Cx35 phosphorylation at night produced the predicted changes in coupling. Thus, it is likely that Cx35 phosphorylation state is causally related to photoreceptor coupling.

In our photoreceptor experiments, PKA activity had parallel effects on both Ser110 and Ser276. The polarity of phosphorylation at these residues was consistent with a direct action of PKA, although an intervening kinase step cannot be ruled out. In some other cell types, PKA action on gap junctions is clearly not direct. In rabbit AII amacrine cells, D_1 dopamine receptor activation and PKA activity uncouple gap junctions by reducing Cx36 phosphorylation through activation of protein phosphatase 2A-like activity (Kothmann et al., 2009). AII amacrine cells follow the behavior of Cx35 transfected in HeLa cells, in which PKA activity reduces coupling (O'Brien et al., 2004; Ouyang et al., 2005); the phosphorylation state of Cx35 and the involvement of a phosphatase have not yet been examined in that model system.

The striking difference in regulation of gap junctional coupling between photoreceptors and AII amacrine cells emphasizes that the signaling pathways that control coupling are specific to each cell type and are likely locally assembled close to the gap junction. Ouyang et al. (2005) observed that a small (7 aa) truncation of the C-terminal tip of Cx35 inverted the polarity of regulation of coupling by PKA activity in HeLa cells. Instead of reducing coupling, as in the wild-type Cx35, PKA activity increased coupling in the truncation mutant in a manner that

required the Ser110 and Ser276 phosphorylation sites, mirroring the behavior we observed in photoreceptors. Given the recent understanding that a protein phosphatase can play a central role in the signaling pathway that reduces coupling (Kothmann et al., 2009), one interpretation of those results is that the truncation mutant changes the association of a phosphatase with Cx35. The PDZ (postsynaptic density-95/Discs large/zonula occludens-1) domain-containing tight junction proteins zonula occludens-1 and zonula occludens-2 have been shown to bind to the C-terminal tip of Cx36 and to be colocalized with Cx36 in the retina (Li et al., 2004; Ciolofan et al., 2006). These scaffolding proteins may provide a matrix for association of appropriate signaling complexes with Cx35/36 and thus may play an integral role in its regulation.

A mutational analysis of Cx35 showed that phosphorylation at both Ser110 and Ser276 was required to achieve the full dynamic range of regulation observed for the wild-type connexin (Ouyang et al., 2005). The effects of the two sites were more than additive, suggesting that a combinatorial form of regulation controls coupling. A number of different protein kinases phosphorylate these sites on Cx35 and Cx36, but the two sites are not equivalent and some protein kinases do not target them equally (Kothmann et al., 2007; Alev et al., 2008). The differences in the two sites and the requirement for multisite regulation establish the potential for several signaling pathways to control coupling. Given the diversity of neurons that are electrically coupled by connexin 36 gap junctions (Connors and Long, 2004), one would expect a number of different signaling pathways to regulate coupling in different neurons via convergence on these two phosphorylation sites.

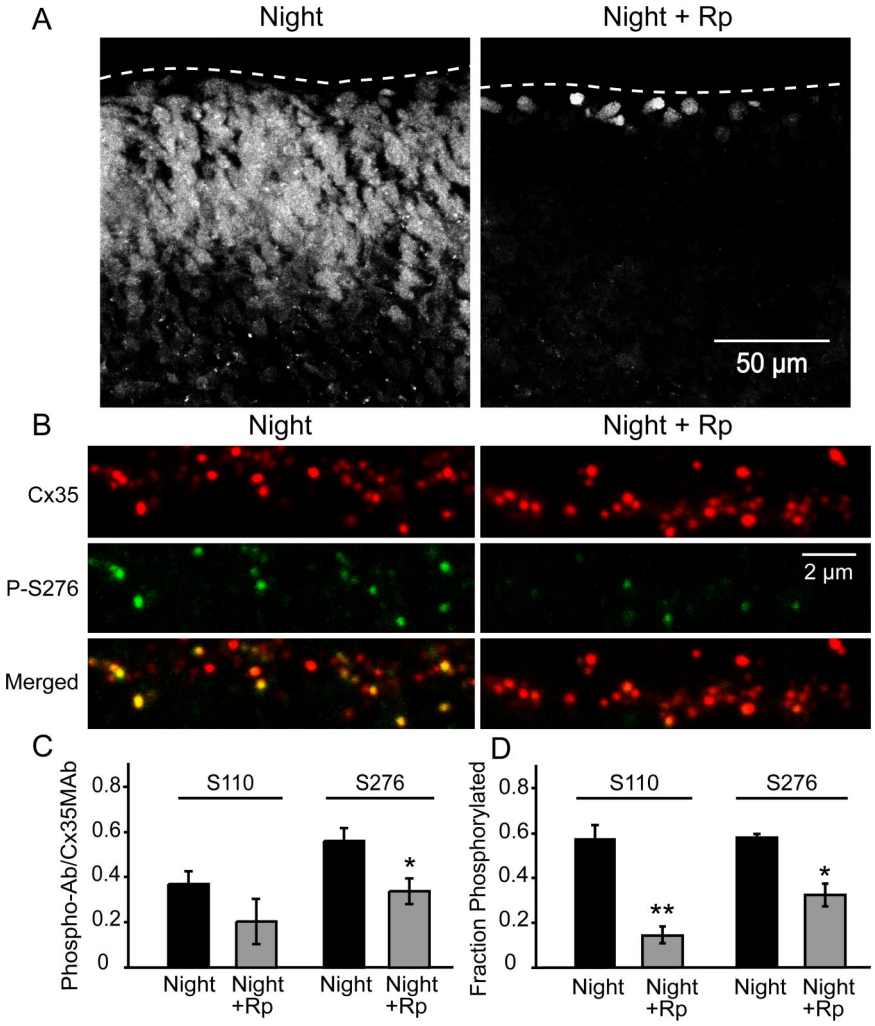

Figure 7. Blocking PKA activity reduces photoreceptor coupling and Cx35 phosphorylation at night. Treatment with the PKA inhibitor Rp-8-cpt-cAMPS (20 μM) in darkness during the night reduced the spread of Neurobiotin through the photoreceptor network (***A***). Rp treatment also reduced Cx35 phosphorylation in the OPL (***B***). Ser276 showed significant reduction in the median ratio of phospho-Cx35 Ab/Cx35 monoclonal Ab labeling intensity (***C***); both Ser110 and Ser276 showed significant reductions in the fraction of Cx35 plaques phosphorylated (***D***). $N = 6$ for Ser110 control and Rp; $n = 6$ for Ser276 control and $n = 4$ for Ser276 Rp. Error bars are $\pm$SEM. *$p < 0.05$; **$p < 0.01$.

Rod–cone and cone–cone coupling

In our experiments, we pooled data from all OPL Cx35 gap junctions because it was not possible to objectively discriminate between cone–cone, rod–cone, rod–rod (if they are present and contain Cx35) and bipolar cell gap junctions. The presence of a small number of gap junctions that were relatively highly phosphorylated during the day may reflect a different population. However, the distributions of phospho-Cx35 labeling intensity during night and day (Fig. 5) did not reveal a separable population of gap junctions.

Uncoupling of rod–cone gap junctions during the daytime contributes to the well documented effect of reducing the influence of rods on signals passing through the cone pathway (Mangel et al., 1994; Wang and Mangel, 1996). The physiological consequences of uncoupling cone–cone gap junctions are less obvious. The modest coupling observed between mammalian cones electrophysiologically (DeVries et al., 2002; Hornstein et al., 2004; Li and DeVries, 2004) most likely represents nearly the minimum coupling corresponding to daytime (Fig. 3) or subjective day (Ribelayga et al., 2008) conditions. This amount of coupling provides a moderate improvement in signal/noise at the synapse with only a modest penalty in loss of spatial acuity and chromatic separation (Hsu et al., 2000; DeVries et al., 2002). Our data imply that cone coupling increases at night, but in scotopic conditions the cone is outside of its operating range. What then is the value of enhanced cone–cone coupling?

One possibility is that cone–cone coupling is essential for rod pathway function. The rod–rod bipolar cell synapse has a very limited dynamic range attributable in part to saturation of components of the rod presynaptic mechanism (Attwell et al., 1987; Sampath and Rieke, 2004) and in part to the nonlinearity of the rod bipolar glutamate receptor transduction mechanism (Field and Rieke, 2002; Sampath and Rieke, 2004), which filters synaptic noise (van Rossum and Smith, 1998). Under conditions in which rods absorb more than a few photons per rod integration time, recruitment of cone synapses via rod–cone electrical coupling provides a mechanism to code increases in light intensity when the rod–rod bipolar pathway is saturated (Hornstein et al., 2005). Enhanced cone–cone coupling under scotopic to mesopic con-

ditions would allow this mechanism to progressively recruit cone synapses as the voltage input from rods increases. Such a mechanism would be achromatic and so would not be hindered by, and in fact would benefit from, indiscriminate coupling among cone types. Additional synaptic mechanisms are present to facilitate information transfer to cone bipolar cells under scotopic conditions. Horizontal cell light responsiveness is reduced via suppression of glutamate receptor currents (Knapp and Dowling, 1987) and horizontal cell spinules are retracted in the dark (Weiler and Wagner, 1984; Djamgoz et al., 1988). Both mechanisms reduce horizontal cell feedback to cone terminals, enabling the transmission of weak signals. A role for cone–cone coupling in scotopic vision could account for the predicted enhancement of cone coupling at night.

References

Alev C, Urschel S, Sonntag S, Zoidl G, Fort AG, Höher T, Matsubara M, Willecke K, Spray DC, Dermietzel R (2008) The neuronal connexin36 interacts with and is phosphorylated by CaMKII in a way similar to CaMKII interaction with glutamate receptors. Proc Natl Acad Sci U S A 105:20964–20969.

Attwell D, Borges S, Wu SM, Wilson M (1987) Signal clipping by the rod output synapse. Nature 328:522–524.

Baylor DA, Fuortes MG, O'Bryan PM (1971) Lateral interaction between vertebrate photoreceptors. Vision Res 11:1195–1196.

Bloomfield SA, Xin D, Persky SE (1995) A comparison of receptive field and tracer coupling size of horizontal cells in the rabbit retina. Vis Neurosci 12:985–999.

Bloomfield SA, Xin D, Osborne T (1997) Light-induced modulation of coupling between AII amacrine cells in the rabbit retina. Vis Neurosci 14:565–576.

Ciolofan C, Li XB, Olson C, Kamasawa N, Gebhardt BR, Yasumura T, Morita M, Rash JE, Nagy JI (2006) Association of connexin36 and zonula occludens-1 with zonula occludens-2 and the transcription factor zonula occludens-1-associated nucleic acid-binding protein at neuronal gap junctions in rodent retina. Neuroscience 140:433–451.

Cohen AI, Blazynski C (1987) Tryptamine and some related molecules block the accumulation of a light-sensitive pool of cyclic AMP in the dark-adapted, dark-incubated mouse retina. J Neurochem 48:729–737.

Cohen AI, Todd RD, Harmon S, O'Malley KL (1992) Photoreceptors of mouse retinas possess D4 receptors coupled to adenylate cyclase. Proc Natl Acad Sci U S A 89:12093–12097.

Connors BW, Long MA (2004) Electrical synapses in the mammalian brain. Annu Rev Neurosci 27:393–418.

Cooper NG, McLaughlin BJ (1981) Gap junctions in the outer plexiform layer of the chick retina: thin section and freeze-fracture studies. J Neurocytol 10:515–529.

Copenhagen DR, Green DG (1987) Spatial spread of adaptation within the cone network of turtle retina. J Physiol 393:763–776.

Cuenca N, Fernández E, García M, De Juan J (1993) Dendrites of rod dominant ON-bipolar cells are coupled by gap junctions in carp retina. Neurosci Lett 162:34–38.

Dang L, Pulukuri S, Mears AJ, Swaroop A, Reese BE, Sitaramayya A (2004) Connexin 36 in photoreceptor cells: studies on transgenic rod-less and cone-less mouse retinas. Mol Vis 10:323–327.

Deans MR, Volgyi B, Goodenough DA, Bloomfield SA, Paul DL (2002) Connexin36 is essential for transmission of rod-mediated visual signals in the mammalian retina. Neuron 36:703–712.

Dearry A, Burnside B (1985) Dopamine inhibits forskolin- and 3-isobutyl-1-methylxanthine-induced dark-adaptive retinomotor movements in isolated teleost retinas. J Neurochem 44:1753–1763.

Dearry A, Burnside B (1986) Dopaminergic regulation of cone retinomotor movement in isolated teleost retinas: I. Induction of cone contraction is mediated by D2 receptors. J Neurochem 46:1006–1021.

Dearry A, Edelman JL, Miller S, Burnside B (1990) Dopamine induces light-adaptive retinomotor movements in bullfrog cones via D2 receptors and in retinal pigment epithelium via D1 receptors. J Neurochem 54:1367–1378.

Degen J, Meier C, Van Der Giessen RS, Söhl G, Petrasch-Parwez E, Urschel S, Dermietzel R, Schilling K, De Zeeuw CI, Willecke K (2004) Expression pattern of lacZ reporter gene representing connexin36 in transgenic mice. J Comp Neurol 473:511–525.

DeVries SH, Baylor DA (1995) An alternative pathway for signal flow from rod photoreceptors to ganglion cells in mammalian retina. Proc Natl Acad Sci U S A 92:10658–10662.

DeVries SH, Qi X, Smith R, Makous W, Sterling P (2002) Electrical coupling between mammalian cones. Curr Biol 12:1900–1907.

Djamgoz MB, Downing JE, Kirsch M, Prince DJ, Wagner HJ (1988) Plasticity of cone horizontal cell functioning in cyprinid fish retina: effects of background illumination of moderate intensity. J Neurocytol 17:701–710.

Field GD, Rieke F (2002) Nonlinear signal transfer from mouse rods to bipolar cells and implications for visual sensitivity. Neuron 34:773–785.

Gold GH, Dowling JE (1979) Photoreceptor coupling in retina of the toad, *Bufo marinus*. I. Anatomy. J Neurophysiol 42:292–310.

Hillman DW, Lin D, Burnside B (1995) Evidence for D4 receptor regulation of retinomotor movement in isolated teleost cone inner-outer segments. J Neurochem 64:1326–1335.

Hornstein EP, Verweij J, Schnapf JL (2004) Electrical coupling between red and green cones in primate retina. Nat Neurosci 7:745–750.

Hornstein EP, Verweij J, Li PH, Schnapf JL (2005) Gap-junctional coupling and absolute sensitivity of photoreceptors in macaque retina. J Neurosci 25:11201–11209.

Hsu A, Smith RG, Buchsbaum G, Sterling P (2000) Cost of cone coupling to trichromacy in primate fovea. J Opt Soc Am A Opt Image Sci Vis 17:635–640.

Kihara AH, Paschon V, Cardoso CM, Higa GS, Castro LM, Hamassaki DE, Britto LR (2009) Connexin36, an essential element in the rod pathway, is highly expressed in the essentially rodless retina of *Gallus gallus*. J Comp Neurol 512:651–663.

Knapp AG, Dowling JE (1987) Dopamine enhances excitatory amino acid-gated conductances in cultured retinal horizontal cells. Nature 325:437–439.

Kolb H (1977) The organization of the outer plexiform layer in the retina of the cat: electron microscopic observations. J Neurocytol 6:131–153.

Kothmann WW, Li X, Burr GS, O'Brien J (2007) Connexin 35/36 is phosphorylated at regulatory sites in the retina. Vis Neurosci 24:363–375.

Kothmann WW, Massey SC, O'Brien J (2009) Dopamine-stimulated dephosphorylation of connexin 36 mediates AII amacrine cell uncoupling. J Neurosci 29:14903–14911.

Krizaj D, Gábriel R, Owen WG, Witkovsky P (1998) Dopamine D2 receptor-mediated modulation of rod-cone coupling in the *Xenopus* retina. J Comp Neurol 398:529–538.

Lamb TD, Simon EJ (1976) The relation between intercellular coupling and electrical noise in turtle photoreceptors. J Physiol 263:257–286.

Larison KD, Bremiller R (1990) Early onset of phenotype and cell patterning in the embryonic zebrafish retina. Development 109:567–576.

Lee EJ, Han JW, Kim HJ, Kim IB, Lee MY, Oh SJ, Chung JW, Chun MH (2003) The immunocytochemical localization of connexin 36 at rod and cone gap junctions in the guinea pig retina. Eur J Neurosci 18:2925–2934.

Li W, DeVries SH (2004) Separate blue and green cone networks in the mammalian retina. Nat Neurosci 7:751–756.

Li X, Olson C, Lu S, Kamasawa N, Yasumura T, Rash JE, Nagy JI (2004) Neuronal connexin36 association with zonula occludens-1 protein (ZO-1) in mouse brain and interaction with the first PDZ domain of ZO-1. Eur J Neurosci 19:2132–2146.

Mangel SC, Baldridge WH, Weiler R, Dowling JE (1994) Threshold and chromatic sensitivity changes in fish cone horizontal cells following prolonged darkness. Brain Res 659:55–61.

Mills SL, Massey SC (1998) The kinetics of tracer movement through homologous gap junctions in the rabbit retina. Vis Neurosci 15:765–777.

Mitropoulou G, Bruzzone R (2003) Modulation of perch connexin35 hemichannels by cyclic AMP requires a protein kinase A phosphorylation site. J Neurosci Res 72:147–157.

Nelson R (1977) Cat cones have rod input: a comparison of the response properties of cones and horizontal cell bodies in the retina of the cat. J Comp Neurol 172:109–135.

Nir I, Haque R, Iuvone PM (2001) Regulation of cAMP by light and dopamine receptors is dysfunctional in photoreceptors of dystrophic retinal degeneration slow(rds) mice. Exp Eye Res 73:265–272.

Nir I, Harrison JM, Haque R, Low MJ, Grandy DK, Rubinstein M, Iuvone PM (2002) Dysfunctional light-evoked regulation of cAMP in photorecep-

tors and abnormal retinal adaptation in mice lacking dopamine D_4 receptors. J Neurosci 22:2063–2073.
O'Brien J, Nguyen HB, Mills SL (2004) Cone photoreceptors in bass retina use two connexins to mediate electrical coupling. J Neurosci 24:5632–5642.
Ouyang X, Winbow VM, Patel LS, Burr GS, Mitchell CK, O'Brien J (2005) Protein kinase A mediates regulation of gap junctions containing connexin35 through a complex pathway. Brain Res Mol Brain Res 135:1–11.
Patel LS, Mitchell CK, Dubinsky WP, O'Brien J (2006) Regulation of gap junction coupling through the neuronal connexin Cx35 by nitric oxide and cGMP. Cell Commun Adhes 13:41–54.
Pierce ME, Besharse JC (1985) Circadian regulation of retinomotor movements. I. Interaction of melatonin and dopamine in the control of cone length. J Gen Physiol 86:671–689.
Raviola E, Gilula NB (1973) Gap junctions between photoreceptor cells in the vertebrate retina. Proc Natl Acad Sci U S A 70:1677–1681.
Raviola E, Gilula NB (1975) Intramembrane organization of specialized contacts in the outer plexiform layer of the retina. A freeze-fracture study in monkeys and rabbits. J Cell Biol 65:192–222.
Rey HL, Burnside B (1999) Adenosine stimulates cone photoreceptor myoid elongation via an adenosine A2-like receptor. J Neurochem 72:2345–2355.
Ribelayga C, Wang Y, Mangel SC (2002) Dopamine mediates circadian clock regulation of rod and cone input to fish retinal horizontal cells. J Physiol 544:801–816.
Ribelayga C, Cao Y, Mangel SC (2008) The circadian clock in the retina controls rod-cone coupling. Neuron 59:790–801.
Sampath AP, Rieke F (2004) Selective transmission of single photon responses by saturation at the rod-to-rod bipolar synapse. Neuron 41:431–443.
Schneeweis DM, Schnapf JL (1995) Photovoltage of rods and cones in the macaque retina. Science 268:1053–1056.
Schneeweis DM, Schnapf JL (1999) The photovoltage of macaque cone photoreceptors: adaptation, noise, and kinetics. J Neurosci 19:1203–1216.
Schwartz EA (1975) Cones excite rods in the retina of the turtle. J Physiol 246:639–651.
Stella SL Jr, Thoreson WB (2000) Differential modulation of rod and cone calcium currents in tiger salamander retina by D2 dopamine receptors and cAMP. Eur J Neurosci 12:3537–3548.
Stella SL Jr, Bryson EJ, Thoreson WB (2002) A2 adenosine receptors inhibit calcium influx through L-type calcium channels in rod photoreceptors of the salamander retina. J Neurophysiol 87:351–360.
Stella SL Jr, Bryson EJ, Cadetti L, Thoreson WB (2003) Endogenous adenosine reduces glutamatergic output from rods through activation of A2-like adenosine receptors. J Neurophysiol 90:165–174.
Stenkamp DL, Iuvone PM, Adler R (1994) Photomechanical movements of cultured embryonic photoreceptors: regulation by exogenous neuromodulators and by a regulable source of endogenous dopamine. J Neurosci 14:3083–3096.
Thoreson WB, Stella SL Jr, Bryson EI, Clements J, Witkovsky P (2002) D2-like dopamine receptors promote interactions between calcium and chloride channels that diminish rod synaptic transfer in the salamander retina. Vis Neurosci 19:235–247.
Tomita T, Kaneko A, Murakami M, Pautler EL (1967) Spectral response curves of single cones in the carp. Vision Res 7:519–531.
Trümpler J, Dedek K, Schubert T, de Sevilla Müller LP, Seeliger M, Humphries P, Biel M, Weiler R (2008) Rod and cone contributions to horizontal cell light responses in the mouse retina. J Neurosci 28:6818–6825.
van Rossum MC, Smith RG (1998) Noise removal at the rod synapse of mammalian retina. Vis Neurosci 15:809–821.
Völgyi B, Deans MR, Paul DL, Bloomfield SA (2004) Convergence and segregation of the multiple rod pathways in mammalian retina. J Neurosci 24:11182–11192.
Wang Y, Mangel SC (1996) A circadian clock regulates rod and cone input to fish retinal cone horizontal cells. Proc Natl Acad Sci U S A 93:4655–4660.
Weiler R, Wagner HJ (1984) Light-dependent change of cone-horizontal cell interactions in carp retina. Brain Res 298:1–9.
Witkovsky P, Shakib M, Ripps H (1974) Interreceptoral junctions in the teleost retina. Invest Ophthalmol 13:996–1009.
Witkovsky P, Stone S, Besharse JC (1988) Dopamine modifies the balance of rod and cone inputs to horizontal cells of the *Xenopus* retina. Brain Res 449:332–336.
Witkovsky P, Stone S, Tranchina D (1989) Photoreceptor to horizontal cell synaptic transfer in the *Xenopus* retina: modulation by dopamine ligands and a circuit model for interactions of rod and cone inputs. J Neurophysiol 62:864–881.
Yang XL, Wu SM (1989) Modulation of rod-cone coupling by light. Science 244:352–354.
Zhang J, Wu SM (2004) Connexin35/36 gap junction proteins are expressed in photoreceptors of the tiger salamander retina. J Comp Neurol 470:1–12.
Zimmerman AL, Rose B (1985) Permeability properties of cell-to-cell channels: kinetics of fluorescent tracer diffusion through a cell junction. J Membr Biol 84:269–283.